Asymmetric Ring-Hybrid Phase Shifters and Attenuators

Hee-Ran Ahn, *Senior Member, IEEE*, and Ingo Wolff, *Fellow, IEEE*

***Abstract*—A new structure of asymmetric ring-hybrid phase shifters and attenuators is presented. Each consists of an asymmetric ring hybrid and reflecting terminations, and it does not have any additional 90° phase delay line for utilizing symmetric reflecting terminations that conventional phase shifters use. To analyze these asymmetric ring-hybrid phase shifters, *normalized impedance ratios* NI_b and NI_d are introduced, and the possibilities to reduce the size of the reflecting terminations are presented. Using the new structure of the asymmetric ring-hybrid phase shifters, asymmetric ring-hybrid attenuators are synthesized. To analyze the attenuators, *normalized resistance ratios* NR_{Lb} and NR_{Ld} are introduced, so that the resistances in the reflection terminations can arbitrarily be determined. On the basis of the derived new structures, a uniplanar asymmetric ring-hybrid -135° phase shifter and a microstrip asymmetric 4-dB attenuator with 45° phase shift have been fabricated and measured. They show good agreement between measured and simulated results and they may be used for impedance transformers besides their original functions.**

***Index Terms*—Asymmetric ring-hybrid attenuators, asymmetric ring-hybrid phase shifters, impedance transformers with defined phase shifts.**

I. Introduction

PHASE shifters have various applications in microwave equipment, such as linearizers, antennas, and so on. The phase shifters using passive four-port power dividers, branch-line hybrids [1], ring hybrids [2], parallel-coupled directional couplers (backward-wave couplers) [3]–[5], and Lange couplers [6], [7] can provide a constant phase shift across their two output ports. So-called 90° couplers, branch-line hybrids, parallel coupled directional couplers, and Lange couplers have the advantage to use symmetric reflecting terminations. However, the branch-line hybrids have narrow bandwidths [8]–[10] and the parallel coupled directional couplers and Lange couplers are not easy to fabricate. In addition to these disadvantages, they need two additional 90° delay lines to realize 180° phase shifters [11]. For the 180° phase shifters, ring hybrids are good candidates. A phase shifter using a ring hybrid was proposed by White [2], but it needs an additional 90° phase delay line to utilize two symmetric reflecting terminations.

Manuscript received February 3, 2001. This work was supported by Deutsche Forschungsgemeinschaft (DFG).

H.-R. Ahn was with the Department of Electrical Engineering, Gerhard-Mercator-University Duisburg, D-47048 Duisburg, Germany. She is now with the Department of Electrical Engineering, Pohang University of Science and Technology, Pohang 790-784, Korea.

I. Woff is with the Department of Electrical Engineering, Gerhard-Mercator-University Duisburg, D-47048 Duisburg, Germany.

Publisher Item Identifier S 0018-9480(02)03031-4.

In this paper, new structures of asymmetric ring-hybrid phase shifters and attenuators are presented. First, a two-port equivalent circuit of an asymmetric ring hybrid is derived by the method suggested in [12] and the scattering matrix of the asymmetric ring hybrid is calculated adopting the process presented in [13]. On the basis of these derived results, the scattering matrix of the asymmetric ring-hybrid phase shifter is calculated and it will be explained why a 90° phase-delay line is not necessary. A conventional phase shifter and an asymmetric ring-hybrid phase shifter suggested in this paper have been simulated and compared for a 180° phase shift. The compared results will demonstrate that the additional 90° phase-delay line not only costs more in size, but also suffers more frequency dependency. The conventional phase shifters use symmetric couplers together with symmetric reflecting terminations [1]–[7]. However, the asymmetric ring-hybrid phase shifter consists of an asymmetric ring hybrid [12], [14] and asymmetric reflecting terminations, and the asymmetric ring hybrids may be terminated by arbitrary impedances. Therefore, the phase shifters composed of the asymmetric ring hybrids may be used as impedance transformers in addition to their original functions.

To analyze the phase shifters, normalized impedance ratios NI_b and NI_d are introduced. Depending on the values of NI_b and NI_d, there are many choices to design the reflecting terminations and to reduce their size. Normally, if the size of microwave components become smaller, their output-performances are degraded in terms of bandwidths [14], [15]. However, even though the reflecting terminations are smaller, the asymmetric ring-hybrid phase shifters produce the same performances with different values of NI_b and NI_d. Therefore, there are merits to design with freedom of choices. On the basis of the analyzed concept, a uniplanar asymmetric ring-hybrid -135° phase shifter terminated by 30 and 60 Ω has been fabricated on Al_2O_3 and measured at the center frequency of 3 GHz.

Additionally, asymmetric ring-hybrid attenuators have been synthesized adopting the asymmetric phase-shifter concept. Two resistances are needed for the attenuator, but the available values of the resistance are limited in microwave integrated circuits (MICs) and hybrid integrated circuits (HICs). To use commercially available resistors, two normalized resistance ratios of NR_{Lb} and NR_{Ld} are introduced. Based on the analyses, 6-dB attenuators with three different phase shifts of -170°, -160°, and -135° are simulated and sub-poles are considered. The sub-poles may be used to increase the bandwidths of these microwave components [16], [17]. A microstrip asymmetric ring-hybrid 4-dB attenuator with 45°

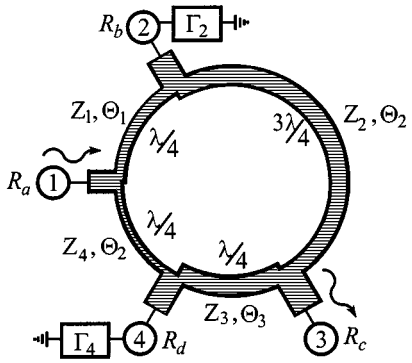

Fig. 1. Asymmetric ring-hybrid phase shifter or attenuator.

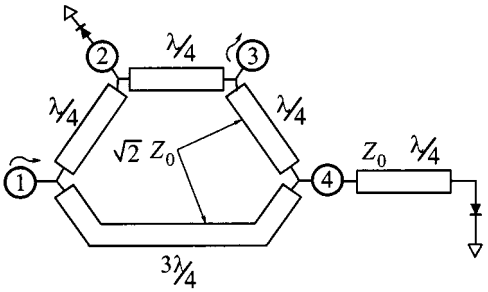

Fig. 2. Conventional ring-hybrid phase shifter using symmetric reflecting terminations.

phase shift terminated by 30 and 60 Ω has been fabricated on Al_2O_3 and measured at the center frequency of 3 GHz. Similar to the asymmetric ring-hybrid phase shifter, the asymmetric ring-hybrid attenuators may be used as impedance transformers because of the asymmetric ring hybrids.

This paper is organized as follows. Section II discusses how to derive the new structure of asymmetric ring-hybrid phase shifters. Section III explains how to derive the design equations of asymmetric ring-hybrid attenuators. Finally, merits in the applications of these phase shifters and attenuators are mentioned in Section IV.

II. Asymmetric Ring-Hybrid Phase Shifters

Fig. 1 shows an asymmetric ring hybrid terminated by arbitrary real impedances R_a, R_b, R_c, and R_d. As this asymmetric ring hybrid has no symmetry planes, even- and odd-mode equivalent circuits cannot be constructed. To derive the scattering parameters, a two-port equivalent circuit is indispensable because the derivation of the scattering parameters may be complicate applying four-port calculations. By the suggested method in [12], the two-port equivalent circuit may easily be derived. With the similar way used in [13], the scattering matrix of the two-port equivalent circuit is calculated (for clarity, refer to the Appendix) and that of the four-port asymmetric ring hybrid is derived by applying the passive properties (reciprocity and unitary condition). In the case of $\Theta_1 = \pi/2$, $\Theta_2 = 3\pi/2$, $\Theta_3 = \pi/2$, and $\Theta_4 = \pi/2$, the scattering parameters of the asymmetric ring hybrid are derived as

$$\boldsymbol{S} = \frac{1}{\sqrt{d_1^2 + d_2^2}} \begin{bmatrix} 0 & -jd_1 & 0 & -jd_2 \\ -jd_1 & 0 & jd_2 & 0 \\ 0 & jd_2 & 0 & -jd_1 \\ -jd_2 & 0 & -jd_1 & 0 \end{bmatrix} \quad (1)$$

where d_1/d_2 is S_{21}/S_{41}.

In the case of conventional ring hybrids [18]–[20], the relative output voltages at the output ports ① and ④ in Fig. 1 are given by $d_1/d_2 = Z_4/Z_1$. For perfect matchings, $(Z_0/Z_1)^2 + (Z_0/Z_2)^2 = 1$ is required, where Z_0 is the system impedance when the ring hybrid is terminated by equal impedances Z_0's. However, for the asymmetric ring hybrid, the output scattering-parameter ratio d_1/d_2 is no longer proportional to the characteristic impedance ratio Z_4/Z_1 and the ratio d_1/d_2 is a function of both the termination impedances R_b, R_d and characteristic impedances Z_4, Z_1 [12]. Therefore, all the characteristic impedances Z_1, Z_2, Z_3, and Z_4 are different from each other and a closed formula for perfect matchings and arbitrary power divisions cannot be introduced in any asymmetric ring hybrids.

If the asymmetric ring hybrid shown in Fig. 1 is terminated by reflection coefficients Γ_2 and Γ_4 at ports ② and ④, respectively, the scattering matrix of the two-port ①–③ is calculated as

$$\boldsymbol{S'} = \frac{1}{{d_1}^2 + {d_2}^2} \begin{bmatrix} -\left(d_1^2\Gamma_2 + d_2^2\Gamma_4\right) & d_1 d_2 \left(\Gamma_2 - \Gamma_4\right) \\ d_1 d_2 \left(\Gamma_2 - \Gamma_4\right) & -\left(d_1^2\Gamma_4 + d_2^2\Gamma_2\right) \end{bmatrix}. \quad (2)$$

Applying perfect matching conditions at port ①, port ③, and reciprocity in (2) results in $d_1 = d_2$. It is straightforward to confirm that if ring hybrids are used for the phase shifters, the ring hybrids must be 3-dB ring hybrids (equal power division). Calculating (2) with the condition $d_1 = d_2$ yields

$$\boldsymbol{S'} = \frac{1}{2} \begin{bmatrix} -(\Gamma_2 + \Gamma_4) & \Gamma_2 - \Gamma_4 \\ \Gamma_2 - \Gamma_4 & -(\Gamma_2 + \Gamma_4) \end{bmatrix}. \quad (3)$$

Fig. 2 shows a ring-hybrid phase shifter proposed by [2]. It requires a $\lambda/4$ phase-shift transmission line between port ④ and a diode. The diode operates as an electronic on–off switch when switched between a fixed forward bias and a reverse bias. Under forward bias, the diode offers a very low impedance, thus approximating a short circuit (on state), and under reverse bias, it offers a very high impedance, approximating an open circuit (off state). Due to the diode characteristics, if the bias condition of one diode at port ② is different from that at port ④, the perfect matching condition $\Gamma_2 = -\Gamma_4$ in (3) can be satisfied without a $\lambda/4$ phase-shift transmission line.

Fig. 3 shows the simulated results of two ring-hybrid phase shifters. "Aps" means "asymmetric ring-hybrid phase shifter" proposed in this paper and "Cps" means "conventional ring-hybrid phase shifter," as shown in Fig. 2. The asymmetric ring-hybrid phase shifter has two diodes at port ② and ④, i.e., a forward-biased diode at port ② and a backward-biased diode at port ④ without any additional $\lambda/4$ transmission line. For the simulations, two ring hybrids have been terminated by equal impedances of 50 Ω and short and open circuits have been used for the forward- and reverse-biased operations of the diodes, respectively. The simulations have been carried out under ideal conditions (e.g., no losses of the transmission lines) and a circuit simulator EEsof Libra has been used. Simulated insertion- and return-loss results are plotted in Fig. 3(a), and the phase responses in Fig. 3(b). If the two-ring hybrid phase shifters are

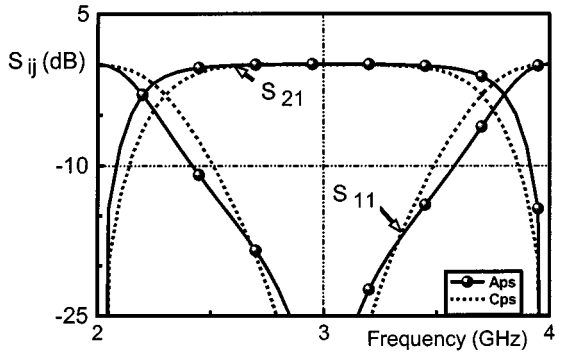

(a)

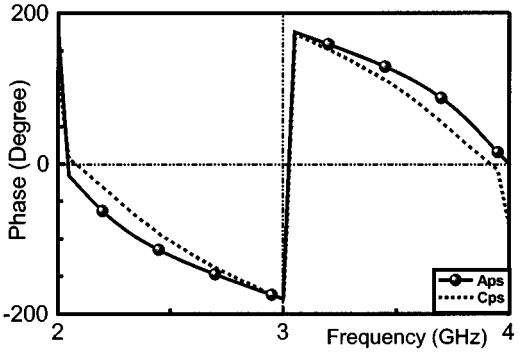

(b)

Fig. 3. Simulated results of an asymmetric and a conventional ring-hybrid phase shifter. (a) Simulated insertion and return loss. (b) Simulated phase responses.

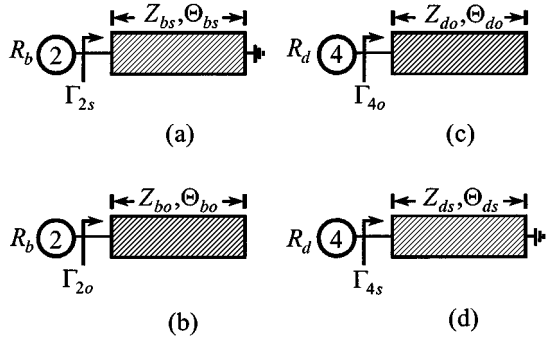

Fig. 4. Simple structures to realize the reflection coefficients Γ_2 and Γ_4. (a) Short-circuited transmission line to realize Γ_2. (b) Open-circuited transmission line to realize Γ_2. (c) Open-circuited transmission line to realize Γ_4. (d) Short-circuited transmission line to realize Γ_4.

compared, both the insertion- and return-loss performances of the "Aps" are better than those of the "Cps." The phase responses of "Aps" are especially less dependent on frequency than those of the "Cps." The simulated results demonstrate that the additional 90° transmission line in Fig. 2 not only costs more in size, but also results in more frequency dependency.

Fig. 4 shows four simple reflecting terminations to realize Γ_2 and Γ_4, where Z_b, Θ_b, Z_d, and Θ_d are the characteristic impedances and the electrical lengths of the transmission lines connected to ports ② and ④, respectively. The subscripts "b" and "d" denote ports ② and ④, respectively, and the subscripts "s" and "o" indicate short- and open-circuited transmission lines, respectively. Therefore, Γ_2, Z_b, and Θ_b become Γ_{2s}, Z_{bs}, and Θ_{bs} when the transmission line connected at port ② is terminated in a short circuit. Γ_2, Z_b, and Θ_b become Γ_{2o}, Z_{bo}, and Θ_{bo} with the open-circuited transmission line and so forth in Fig. 4.

The scattering parameter S_{21} in (3) is Γ_2 under the perfect matching condition $\Gamma_2 = -\Gamma_4$. The angle of Γ_2, Θ is derived as follows. In the case of $0° \le \Theta_{bs} \le 90°$ in Fig. 4(a):

$$\Theta = \mathrm{Ang}\,(\Gamma_2 = \Gamma_{2s}) \tag{4}$$

where $\Gamma_2 = \Gamma_{2s} = (jNI_{bs}\tan\Theta_{bs} - 1)/(jNI_{bs}\tan\Theta_{bs} + 1)$ with $NI_{bs} = Z_{bs}/R_b$. In the case of $0° \le \Theta_{bo} \le 90°$ in Fig. 4(b)

$$\Theta = \mathrm{Ang}\,(\Gamma_2 = \Gamma_{2o}) \tag{5}$$

where $\Gamma_2 = \Gamma_{2o} = (jNI_{bo} + \tan\Theta_{bo})/(jNI_{bo} - \tan\Theta_{bo})$ with $NI_{bo} = Z_{bo}/R_b$.

Fig. 5 shows the response curves of Θ versus Θ_{bs}, Θ versus Θ_{bo} and Θ versus NI_{bs} or NI_{bo} on the basis of (4) and (5). The variations in Θ of the reflecting termination in Fig. 4(a) are described in Fig. 5(a), and those with the circuit in Fig. 4(b) are plotted in Fig. 5(b). Fig. 5(c) explains the changes in Θ with several equal electrical lengths $\Theta_{bs} = 22.5°$, 45°, 67.5°, $\Theta_{bo} = 67.5°$, 45°, and 22.5°, when NI_{bs} or NI_{bo} are varied. More detailed data for each figure are given in Tables I–III, respectively. In the case of $NI_{bs} = NI_{bo} = 1$ in Fig. 5(a) and (b), the responses are linear, but as NI_{bs} and NI_{bo} deviate from unit, they show more nonlinear characteristics. Therefore, the phase Θ is dependent on not only Θ_{bs} and Θ_{bo}, but also NI_{bs} and NI_{bo}. The response curves with NI_{bs}'s and those with $(1/NI_{bs})$'s are symmetric about the line with $NI_{bs} = 1$ in Fig. 5(a). The same results coincide with NI_{bo}'s in Fig. 5(b). Depending on which phase shifter is designed, the reflecting termination at port ② is determined referring to Fig. 5(a)–(c) and Tables I–III.

To realize the perfect matching condition $\Gamma_2 + \Gamma_4 = 0$, four pairs, i.e., (a)–(c), (a)–(d), (b)–(c), and (b)–(d) in Fig. 4, are possible. However, the desirable combinations for small-sized reflecting terminations are the pairs (a)–(c) for $0° \le \Theta_{bs} \le 90°$ and (b)–(d) for $0° \le \Theta_{bs} \le 90°$. The formulas for Z_d and Θ_d in Fig. 4(c) or (d) are for $0° \le \Theta_{bs} \le 90°$

$$NI_{do}\cot\Theta_{do} = \frac{1}{NI_{bs}\tan\Theta_{bs}}, \qquad \text{where } NI_{do} = \frac{Z_{do}}{R_d} \tag{6}$$

and for $0° \le \Theta_{bo} \le 90°$

$$NI_{ds}\cot\Theta_{ds} = \frac{1}{IN_{bo}\tan\Theta_{bo}}, \qquad \text{where } NI_{ds} = \frac{Z_{ds}}{R_d}. \tag{7}$$

If $NI_{bs}\cdot NI_{do} = 1$ in (6), Θ_{bs} is always equal to Θ_{do}, and $\Theta_{bo} = \Theta_{ds}$ is valid for $NI_{bo}\cdot NI_{ds} = 1$ in (7). In (4)–(7), NI_{do}, NI_{bs}, NI_{bo}, and NI_{ds} are arbitrary real positive constants, which can be determined depending on the design situations in Tables I and II. In addition to the normalized impedance ratios, the termination impedances of the asymmetric ring hybrid in Fig. 1 may be arbitrarily determined. Therefore, the asymmetric ring-hybrid phase shifter may be used as impedance transformers in addition to the phase shifters, and there are so many design choices for these asymmetric components.

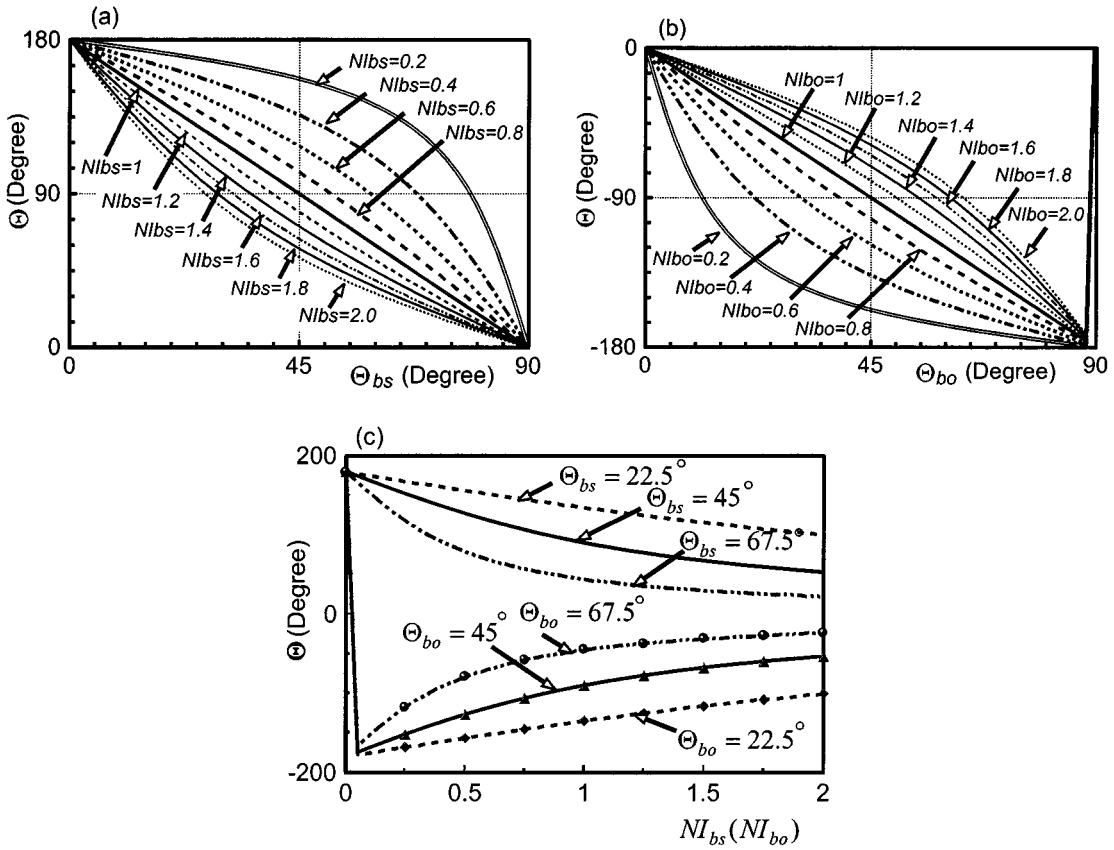

Fig. 5. Phase responses depending on NI_b and Θ_b. (a) Phase responses depending on Θ_{bs} and NI_{bs}. (b) Phase responses depending on Θ_{bo} and NI_{bo}. (c) Phase responses with three Θ_{bs}'s and Θ_{bo}'s depending on NI_b.

TABLE I
ANGLE OF Γ_2, Θ DEPENDING ON NI_{bs} AND Θ_{bs}

Θ_{bs} \ NI_{bs}	0.2	0.4	0.6	0.8	1	1.2	1.4	1.6	1.8	2.0
Θ=180°	0°	0°	0°	0°	0°	0°	0°	0°	0°	0°
Θ=157.5°	44.8°	26.4°	18.3°	13.96°	11.3°	9.41°	8.09°	7.09°	6.31°	5.68°
Θ=135.0°	64.2°	46.0°	34.6°	27.4°	22.5°	19.0°	16.5°	14.5°	12.96°	11.7°
Θ=112.5°	73.3°	59.1°	48.1°	39.9°	33.6°	29.1°	25.5°	22.7°	20.4°	18.5°
Θ=90.0°	78.7°	68.2°	59.0°	51.3°	45°	39.8°	35.5°	32.0°	29.1°	26.6°
Θ=67.5°	82.4°	75.0°	68.2°	61.9°	56.3	51.3°	46.9°	43.1°	39.7°	36.8°
Θ=45.0°	85.3°	80.6°	76.0°	71.7°	67.5	63.6°	59.9°	56.5°	53.3°	50.4°
Θ=22.5°	87.7°	85.5°	83.2°	80.96°	78.75	76.58°	74.4°	72.3°	70.3°	68.3°
Θ=0°	90°	90°	90°	90°	90°	90°	90°	90°	90°	90°

There are many possible ways to design an asymmetric ring-hybrid phase shifter. One recommendable design process is as follows.

Step 1) The first step is to determine the termination impedances R_a, R_b, R_c, and R_d depending on design situations. When $R_b = R_d$, the relations of $Z_1 = Z_4$ and $Z_2 = Z_3$ always hold regardless of any values of R_a and R_c. Under the condition of $R_b = R_d$, to determine the value of R_b and R_d as $\sqrt{R_a R_c}$ is recommendable.

Step 2) The second step is to design Γ_2 at port ② for a required phase shift based on (4) and (5) referring to Fig. 5(a) and (b), Table I, or Table II.

Step 3) The last step is to design Γ_4 at port ④ in Fig. 4(c) or (d) for the perfect matching condition. Since the response curves with NI_{bs}'s and those with $(1/NI_{bs})$'s are symmetric about the line with $NI_{bs} = 1$ in Fig. 5(a), it is important to have the relation of $NI_{do} \cdot NI_{bs} = 1$ in designing Γ_4 in Fig. 4(c). In the case of NI_{bo}'s and $(1/NI_{bo})$'s, the

TABLE II
ANGLE OF Γ_2, Θ DEPENDING ON NI_{bo} AND Θ_{bo}

Θ_{bo} \ NI_{bo}	0.2	0.4	0.6	0.8	1	1.2	1.4	1.6	1.8	2.0
Θ=0°	0°	0°	0°	0°	0°	0°	0°	0°	0°	0°
Θ=-22.5°	2.28°	4.55°	6.8°	9.0°	11.3°	13.4°	15.6°	17.7°	19.7°	21.7°
Θ=-45.°	4.74°	9.41°	13.96°	18.33°	22.5°	26.43°	30.10°	33.53°	36.71°	39.64°
Θ=-67.5°	7.61°	14.96°	21.85°	28.13°	33.75°	38.72°	43.09°	46.91°	50.26°	53.19°
Θ=-90.0°	11.3°	21.80°	30.96°	38.66°	45°	50.19°	54.46°	57.99°	60.95°	63.44°
Θ=-112.5°	16.7°	30.91°	41.92°	50.13°	56.25°	60.89°	64.49°	67.33°	69.63°	71.53°
Θ=-135.0°	25.8°	44.00°	55.38°	62.63°	67.5°	70.96°	73.52°	75.49°	77.04°	78.30°
Θ=-157.5°	45.2°	63.56°	71.66°	76.04°	78.75°	80.59°	81.91°	82.91°	83.69°	84.32°
Θ=-180°	90°	90°	90°	90°	90°	90°	90°	90°	90°	90°

TABLE III
CHANGES IN Θ FOR CONSTANT ELECTRICAL LENGTHS Θ_{bs} AND $\Theta_{bo} = 22.5°$, 45°, AND 67.5° VERSUS NI_{bs} AND NI_{bo}

Θ

Θ_{bs} \ NI_{bs}	1/1.9	1/1.6	1/1.3	1	1.3	1.6	1.9
22.5°	155.4°	150.97°	144.65°	135°	123.4°	112.93	103.59°
45°	124.48°	115.99°	104.86°	90.°	75.14°	64.01°	55.51°
67.5°	76.41°	67.07°	56.60°	45.°	35.35°	29.03°	24.60°

Θ

Θ_{bo} \ NI_{bo}	1/1.9	1/1.6	1/1.3	1	1.3	1.6	1.9
67.5°	-155.40°	-150.97°	-144.65°	-135.°	-123.40°	-112.93°	-103.59°
45°	-55.52°	-64.01°	-75.14°	-90.°	-104.86°	-115.99°	-124.48°
22.5°	-24.60°	-29.03°	-35.35°	-45°	-56.60°	-67.07°	-76.41°

relation of $NI_{bo} \cdot NI_{ds} = 1$ is also important for designing Γ_4 in Fig. 4(d).

A. Uniplanar Asymmetric Ring Hybrid $-135°$ Phase Shifter

If a $-135°$ phase shifter terminated in 30 and 60 Ω is needed, let $R_b = R_d$ be $\sqrt{30 \cdot 60} = 42.4\ \Omega$, then $Z_1 = Z_4 = 50.5\ \Omega$ and $Z_2 = Z_3 = 71.4\ \Omega$. The circuit to realize Γ_2 for the $-135°$ phase shifter is that in Fig. 4(a) based on Fig. 5(a) and Table I because the required phase shift is a negative sign of Θ. As NI_{bs} increases, the length of Θ_{bs} becomes shorter. Several cases for the $-135°$ phase shift are written in Table IV together with the data of the ring hybrid. Any case with changes in NI_{bs} produces the same output performance and the experimental data for the case of $NI_{bs} = 1.2$ are given in Table V. This uniplanar phase shifter has been realized on the Al_2O_3 substrate ($\varepsilon_r = 9.9$ and $h = 635\ \mu$m) in coplanar waveguide (CPW) technology and designed at the center frequency of 3 GHz. This uniplanar phase shifter is terminated in 30 and 60 Ω. Therefore, two quarter-wave transformer lines Z_{01} and Z_{03} given in Table V are needed for measuring. The circuit layout for the measurement is depicted in Fig. 6 and measured and predicted results are plotted in Fig. 7.

TABLE IV
SEVERAL DIFFERENT CHOICES TO DESIGN AN ASYMMETRIC RING-HYBRID $-135°$ PHASE SHIFTER

Ring Hybrid				
T. Imp. [Ω]	R_a	R_b	R_c	R_d
	30	42.4	60	42.4
C. Imp [Ω]	Z_1	Z_2	Z_3	Z_4
	50.5	71.4	71.4	50.5
-135° Phase Shift, Z_{bs} and Z_{do} [Ω]				
NI_{bs}	Z_{bs}	Θ_{bs}/°	NI_{do}	Z_{do}	Θ_{do}/°
2	84.8	11.7	0.5	21.2	11.7
1.8	76.4	12.96	0.55	23.6	12.96
1.6	67.9	14.5	0.63	26.5	14.5
1.4	59.4	16.5	0.71	30.3	16.5
1.2	50.9	19.0	0.83	35.4	19.0
1	42.4	22.5	1	42.4	22.5

III. ASYMMETRIC RING-HYBRID ATTENUATOR WITH PHASE SHIFTS

If the magnitude of Γ_2 in (3) is less than unit, the ring-hybrid phase shifter in Fig. 1 is an attenuator. Simple circuits to

TABLE V
FABRICATION DATA OF A UNIPLANAR ASYMMETRIC RING-HYBRID -135° PHASE SHIFTER WITH $NI_{bs} = 1.2$

Ring Hybrid; Z_{01} = 38.7 Ω, Z_{03} = 54.8 Ω Phase shift for Γ_{2s} and Γ_{4o}; Z_{bs} and Z_{do}.			
Z_{01} [μm]	Z_{03} [μm]	$Z_1 = Z_4$ [μm]	Z_2 [μm]
w ; 583 g ; 100 l ; 11059	w ; 334 g ; 200 l ; 10994	w ; 324 g ; 150 l ; 10950	w ; 125 g ; 200 l ; 32635
Z_3 [μm]	Z_{bs} [μm]	Z_{do} [μm]	Z_1 50.5 Ω
w ; 125 g ; 200 l ; 10878	w ; 444 g ; 200 l ; 2337	w ; 896. g ; 100 l ; 2375	Z_2 71.5 Ω

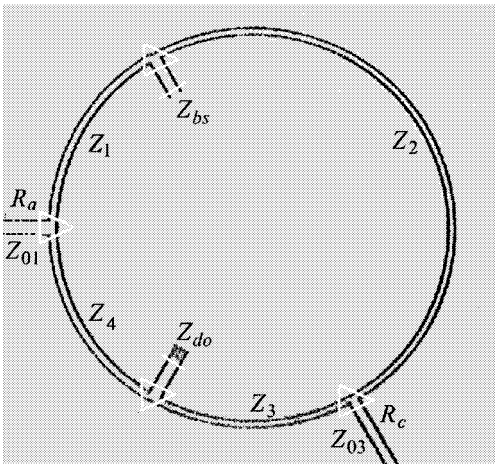

Fig. 6. Layout of a uniplanar asymmetric ring-hybrid -135° phase shifter terminated by 30 and 60 Ω.

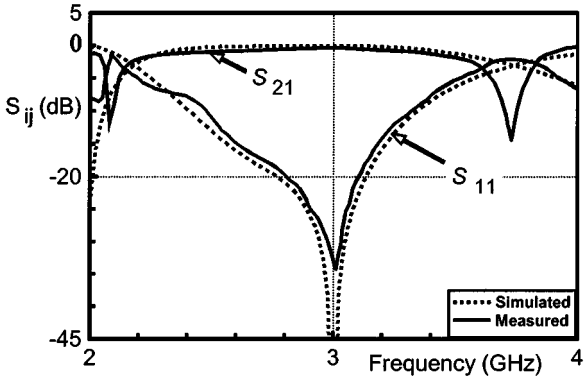

Fig. 7. Measured and predicted results of a uniplanar asymmetric -135° phase shifter.

realize Γ_2 and Γ_4 for an asymmetric ring-hybrid attenuator are depicted in Fig. 8. Each transmission line with the characteristic impedances Z_{ba} or Z_{da} is terminated by R_{Lb} or R_{Ld} instead of a short or an open circuit in Fig. 4. In the case of $NI = 1$ (e.g.,

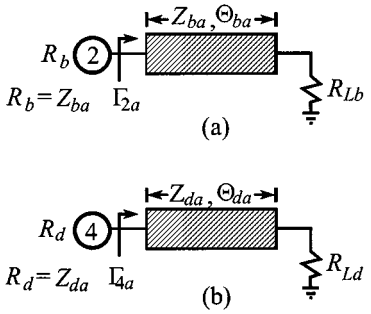

Fig. 8. Simple circuits to realize the reflection coefficients Γ_{2a} and Γ_{4a}. (a) Simple circuit for Γ_{2a}. (b) Simple circuit for Γ_{4a}.

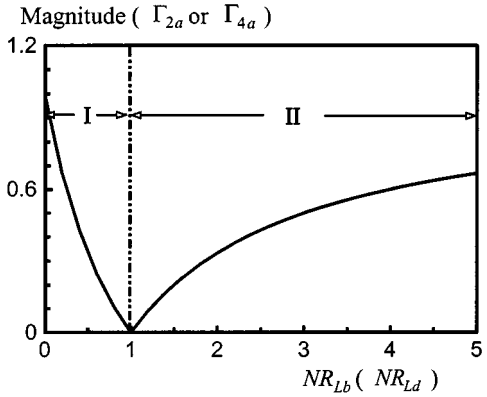

Fig. 9. Magnitude of Γ_{2a} or Γ_{4a} depending on NR_{Lb} or NR_{Ld}.

$R_b = Z_{ba}$ and $R_d = Z_{da}$) for easy analyses, the reflection coefficients Γ_{2a} and Γ_{4a} are calculated as

$$\Gamma_2 = \Gamma_{2a} = \frac{(NR_{Lb}-1) - j\,(NR_{Lb}-1)\tan\Theta_{ba}}{(NR_{Lb}+1) + j\,(NR_{Lb}+1)\tan\Theta_{ba}} \tag{8}$$

where $NR_{Lb} = R_{Lb}/Z_{ba}$ and $R_b = Z_{ba}$ and

$$\Gamma_4 = \Gamma_{4a} = \frac{(NR_{Ld}-1) - j\,(NR_{Ld}-1)\tan\Theta_{da}}{(NR_{Ld}+1) + j\,(NR_{Ld}+1)\tan\Theta_{da}} \tag{9}$$

where $NR_{Ld} = R_{Ld}/Z_{da}$ and $R_d = Z_{da}$. Therefore, the magnitudes of Γ_2 and Γ_4 are

$$\mathrm{Mag}\,(\Gamma_{2a}) = \left|\frac{NR_{Ld}-1}{NR_{Ld}+1}\right| \tag{10}$$

$$\mathrm{Mag}\,(\Gamma_{4a}) = \left|\frac{NR_{Lb}-1}{NR_{Lb}+1}\right|. \tag{11}$$

Also, the angle of $\Gamma_2 = \Gamma_{2a}$ results in, in the case of $0 < NR_{Lb} < 1$

$$Ang\,(\Gamma_{2a}) = \Theta, \qquad \text{with } NI_{bs} = 1 \tag{12}$$

and in the case of $NR_{Lb} > 1$

$$\mathrm{Ang}\,(\Gamma_{2a}) = \Theta, \qquad \text{with } NI_{bo} = 1. \tag{13}$$

On the basis of (10) and (11), the magnitude response of Γ_{2a} or Γ_{4a} is plotted in Fig. 9, where region I is defined by $0 < NR_{Lb} < 1$ or $0 < NR_{Ld} < 1$, and region II is defined by $NR_{Lb} > 1$ or $NR_{Ld} > 1$. There are two values of NR_{Lb} to satisfy a certain attenuation, one is in region I and another

TABLE VI
VALUES OF NR_{Lb} IN REGION I (FIG. 9) FOR GIVEN ATTENUATIONS

Atten. [dB]	NR_{Lb}	Atten. [dB]	NR_{Lb}
1	0.05750	8	0.43050
2	0.11462	9	0.47621
3	0.17099	10	0.51949
4	0.22627	11	0.56025
5	0.28012	12	0.59847
6	0.33227	13	0.63415
7	0.38247	14	0.66732

in region II. However, the output signals with the two different values of NR_{Lb} have a 180° phase difference and one value is always reciprocal to the other one. The same situation coincides with the two different values of NR_{Ld}. The values of NR_{Lb} depending on the attenuations in decibels are given in Table VI.

On the basis of the calculated values given in Table VI, three 6-dB attenuators with different phase shifts, i.e., −170°, −160°, and −135°, have been simulated. They are terminated by two different impedances of 40 and 60 Ω. The values of Θ for −170°, −160°, and −135° phase shift are 170°, 160°, and 135° with $NI_{bs} = 1$ in Fig. 5(a), and NR_{Lb} is located in region I ($0 < NR_{Lb} < 1$) in Fig. 9 from (12). Therefore, NR_{Lb} for the 6-dB attenuation with the phase shifts is 0.3327 from Table VI. From the relation of $NR_{Lb} = R_{Lb}/R_b$ in (8), if a commercially available resistor 15 Ω is used for the R_{Lb}, the termination impedance R_b will be 45.14 Ω. The value of NI_{Ld} is the reciprocal to NR_{Lb} or (1/0.33227) to satisfy the perfect matching condition $\Gamma_2 + \Gamma_4 = 0$. When a commercial resistor 150 Ω is utilized for the R_{Ld}, the termination impedance R_d will be 49.84 Ω. In the case of the 6-dB attenuators, the electrical lengths Θ_{ba}'s for the −170°, −160°, and −135° phase shifts are 5°, 10°, and 22.5°, respectively, from (12), Fig. 5(a) and Table I with $NI_{bs} = 1$. These 6-dB attenuators are terminated by 40 and 60 Ω. Therefore, two quarter-wave transformer lines to transform the termination impedances 40 and 60 Ω to 50 Ω's are needed for measuring. Fig. 10 shows the simulated results of the three attenuators with the −170°, −160°, and −135° phase shift. The insertion loss and matching characteristics for the three attenuators are plotted in Fig. 10(a) and the phase responses in Fig. 10(b). These attenuators are designed at center frequency of 3 GHz and the simulated results of the insertion losses are all −6 dB and return-loss responses are −157.4 dB, −156.4 dB, and −154.4 dB at 3 GHz. The phase responses of the three attenuators are −10°, −20°, and −45° at the center frequency of 3 GHz in Fig. 10(b) because two 90° impedance transformer lines are connected at input and output ports. "Sub-poles" identified in Fig. 10(b) are the kinds of poles that appear when the length of Θ_{ba} is not zero. With an increase in the length of Θ_{ba}, the pole appears farther from the center frequency of 3 GHz. The Θ_{ba} for the −170°, −160°, and −135° phase shifter are 5°, 10°, and 22.5° and the sub-poles appear at 2.87, 2.75, and 2.48 GHz, respectively. How far the sub-pole appears from the design center frequency is not linear and depends on the several parameters, e.g., the length of Θ_{ba}, the input- and output-termination impedances, the resistances of R_{Lb} and R_{Ld}, and so on. Therefore, the pole position and dependence on the parameters may be used to increase the bandwidths. [16], [17].

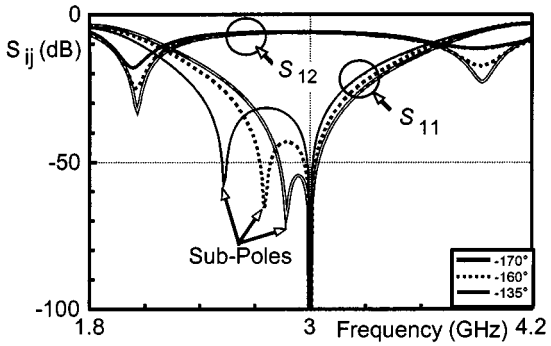

(a)

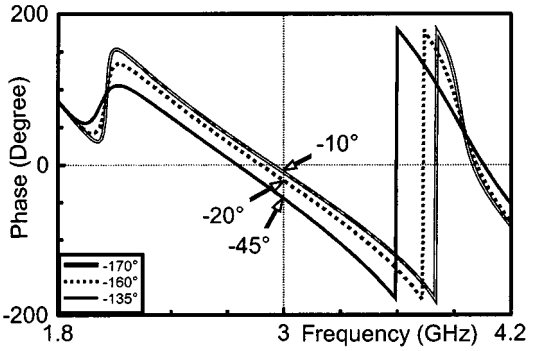

(b)

Fig. 10. Asymmetric ring-hybrid 6-dB attenuators with three different phase shifts −170°, −160°, and −135°. (a) Simulated insertion losses and return losses. (b) Simulated phase responses.

A. Microstrip Asymmetric Ring-Hybrid 4-dB Attenuator With 45° Phase Shift

45° phase shifters have been used to reduce the harmonics of high-power amplifiers and oscillators [21]. On the basis of the derived design (10)–(13) and Table VI, a microstrip asymmetric ring-hybrid 4-dB attenuator with a 45° phase shift has been realized on an Al_2O_3 substrate ($\varepsilon_r = 9.9$ and $h = 635$ μm) and measured at the center frequency of 3 GHz. The NR_{Lb} for 4-dB attenuation is reciprocal to the value in Table VI because the NR_{Lb} for the 45° phase shift must be located in region II in Fig. 9. For the case of $NR_{Lb} = (1/0.22627)$ or 4.4195, if a commercially available resistor 221 Ω is used for the R_{Lb}, R_b is 50 Ω and NR_{Ld} is 0.22627 to satisfy the perfect matching condition. When a commercial resistor 12 Ω is chosen for the R_{Ld}, then R_d is 53.0 Ω. If the microstrip attenuator is terminated in $R_a = 30$ Ω and $R_c = 60$ Ω, all needed characteristic impedances of the transmission lines in Fig. 1 are $Z_1 = 54.65$ Ω, $Z_2 = 77.5$ Ω, $Z_3 = 79.75$ Ω, and $Z_4 = 56.4$ Ω. The electrical lengths of Θ_{ba} and Θ_{da} are equally 22.5° and all necessary data for the fabrication of a microstrip attenuator are given in Table VII, where Z_{01} and Z_{03} are the characteristic impedances of two 90° transformer lines to transform 30 and 60 Ω to 50 Ω's for the measuring. The attenuator with a package is illustrated in Fig. 11(a) and the attenuator itself is expanded in Fig. 11(b). Measured and expected results are plotted in Fig. 12. They show good agreement in the bandwidth where

TABLE VII
FABRICATION DATA FOR A MICROSTRIP ASYMMETRIC RING-HYBRID 4-dB ATTENUATOR WITH 45° PHASE SHIFT. w: CENTER CONDUCTOR, l: LENGTH OF MICROSTRIP LINE

45° phase shift with 4 dB attenuation $\rightarrow NR_{Lb} = 4.4195$ $R_{Lb} = 221\ \Omega \rightarrow R_b = 50.00\ \Omega$, $NR_{Ld} = 0.2263 \rightarrow R_{Ld} = 12\ \Omega$ $\rightarrow R_d = 53.0\ \Omega$.		
Ring Hybrid and Reflection Termination		
$Z_1 = 54.7\ \Omega$	$Z_2 = 77.5\ \Omega$	$Z_3 = 79.8\ \Omega$
$w = 501$ $l = 9736$	$w = 202.3$ $l = 29996$	$w = 185$ $l = 10018$
$Z_4 = 56.4\ \Omega$	$Z_{ba} = 49.8\ \Omega$	$Z_{da} = 53.0\ \Omega$
$w = 468$ $l = 9562$	$w = 613$ $l = 2414$	$w = 537$ $l = 2427$
$Z_{01} = 38.7\ \Omega$	$Z_{03} = 54.8\ \Omega$	
$w = 988$ $l = 9433$	$w = 499$ $l = 9738$	

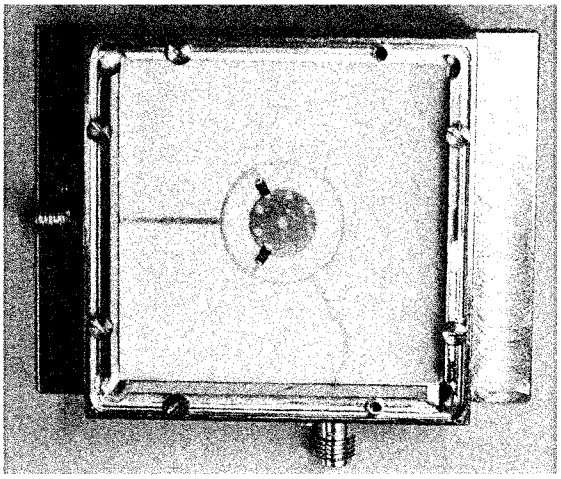

(a)

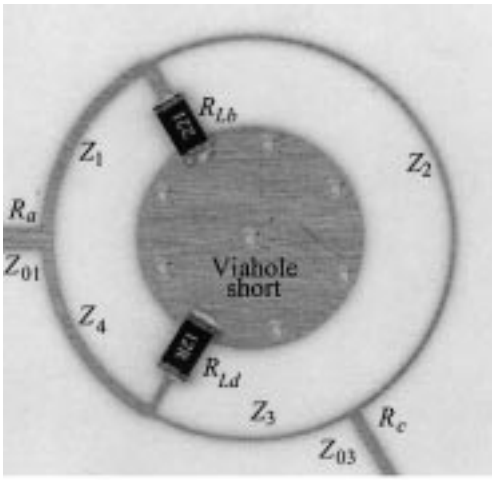

(b)

Fig. 11. Layout for an asymmetric ring-hybrid 4-dB attenuator with 45° phase shift. (a) The microstrip attenuator with a package. (b) The center of the attenuator is expanded.

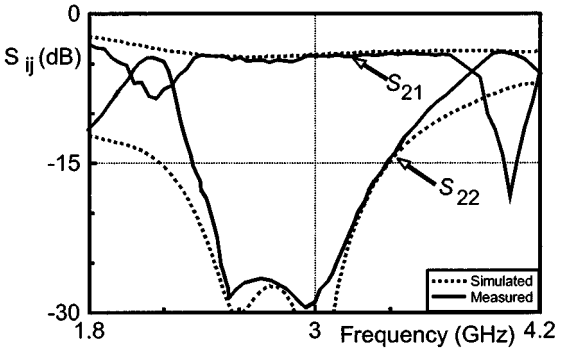

Fig. 12. Measured and simulated results of the asymmetric ring-hybrid 4-dB attenuator with 45° phase shift.

return losses are less than −15 dB. Band-stop characteristics appear in two regions around 2.16 and 4.04 GHz. These band-stop responses are caused by parasitic capacitance and inductance due to soldering resistors on the substrate. These parasitic components take effect depending on frequencies, and the band-stop characteristics at 4.04 GHz appear definitely compared to those at 2.16 GHz. The similar phenomena appears in the case of the uniplanar −135° phase shifter in Fig. 7. The uniplanar phase shifter in Fig. 6 and the microstrip attenuator have been fabricated on an Al_2O_3 substrate. To measure phase responses, the length of feeding lines at input and output ports must be equal to each other. To fabricate the equal feeding lines at the input and output ports, the substrate must be cut in round form. However, there is no way to cut and measure in this way. Therefore, there are no measured phase results in both Figs. 7 and 12.

IV. CONCLUSION

New structures of asymmetric ring-hybrid phase shifters and attenuators have been presented. To analyze these components, the normalized impedance ratios NI_b and NI_d and the normalized resistance ratios NR_{Lb} and NR_{Ld} have been introduced. The NI_b, NI_d, NR_{Lb} and NR_{Ld} are functions of the two termination impedances, the characteristic impedances of the transmission lines connected at the two ports and the resistors for the attenuators. Therefore, many design choices have been given. Additionally, these asymmetric components may be used as impedance transformers together with their original functions.

APPENDIX

When the power is excited at port ①, as shown in Fig. 1, a two-port equivalent circuit may be derived as [12]. The admittance matrix $\boldsymbol{Y}$ of a network $[N]$ and the reference admittance matrix $\boldsymbol{y}$ between ports ① and ② in Fig. 13 are given as

$$\boldsymbol{Y} = \frac{1}{Z_1 j \sin\Theta_1} \begin{bmatrix} \dfrac{jZ_1}{Z_{\text{in}}} \sin\Theta_1 + \cos\Theta_1 & -1 \\ -1 & \cos\Theta_1 \end{bmatrix} \quad \text{(A1)}$$

where $Z_{\text{in}} = Z_4(R_d + jZ_4 \tan\Theta_4)/(Z_4 + jR_d \tan\Theta_4)$

$$\boldsymbol{y} = \begin{bmatrix} \dfrac{1}{R_a} & 0 \\ 0 & \dfrac{1}{R_b} \end{bmatrix}.$$

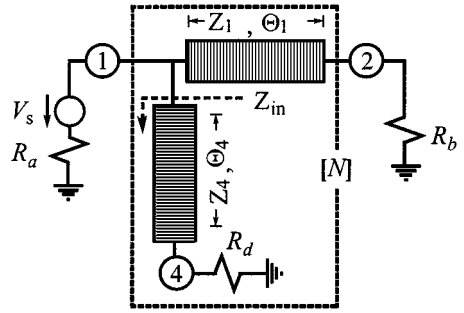

Fig. 13. Two-port equivalent circuit of the asymmetric ring hybrid with a port ① -excitation.

The voltage-based scattering matrix is expressed as $\boldsymbol{S}^v = -(\boldsymbol{Y}+\boldsymbol{y})^{-1}(\boldsymbol{Y}-\boldsymbol{y}^*)$ and if expressing the voltage-based scattering matrix in more detail, it follows that

$$S_{11}^v = -\frac{1}{\Delta_y}\Big[(Y_{11}-y_{11^*})(Y_{22}+y_{22}) - Y_{12}Y_{21}\Big] \quad \text{(A2)}$$

$$S_{12}^v = -\frac{1}{\Delta_y}Y_{12}(y_{22}+y_{22^*}) \quad \text{(A3)}$$

$$S_{21}^v = -\frac{1}{\Delta_y}Y_{21}(y_{11}+y_{11^*}) \quad \text{(A4)}$$

$$S_{22}^v = -\frac{1}{\Delta_y}\Big[(Y_{11}+y_{11})(Y_{22}-y_{22^*}) - Y_{12}Y_{21}\Big] \quad \text{(A5)}$$

where

$$\Delta_y = Y_{11}Y_{22} + Y_{11}y_{22} - Y_{12}Y_{21} + Y_{22}y_{11} + y_{11}y_{22}. \quad \text{(A6)}$$

The relations between basis-independent scattering parameters and the voltage-based ones under the assumption of real reference admittances are

$$S_{11} = S_{11}^v \quad \text{(A7)}$$

$$S_{12} = S_{12}^v\sqrt{\frac{\mathrm{Re}(y_{11})}{\mathrm{Re}(y_{22})}} \quad \text{(A8)}$$

$$S_{21} = S_{21}^v\sqrt{\frac{\mathrm{Re}(y_{22})}{\mathrm{Re}(y_{11})}} \quad \text{(A9)}$$

$$S_{22} = S_{22}^v. \quad \text{(A10)}$$

When $\Theta_1 = \Theta_4 = \pi/2$ in (A1), the network admittance matrix is

$$Y = \begin{bmatrix} Y_{\mathrm{in}} & jY_1 \\ jY_1 & 0 \end{bmatrix}, \qquad \text{where } Y_1 = \frac{1}{Z_1},\ Y_{\mathrm{in}} = \frac{R_d}{Z_4^2}. \quad \text{(A11)}$$

Δ_y and the voltage-based scattering parameter S_{12}^v from (A3), (A6), and (A11) are

$$\Delta_y = \frac{2}{R_a R_b}$$

$$S_{12}^v = -j\sqrt{\frac{d_1^2}{d_1^2+d_2^2}}\sqrt{\frac{R_a}{R_b}}. \quad \text{(A12)}$$

From the relation between S_{12}^v and S_{12} in (A8), the basis-independent scattering parameter S_{12} is

$$S_{12} = -j\sqrt{\frac{d_1^2}{d_1^2+d_2^2}}. \quad \text{(A13)}$$

In a similar way, the scattering matrix of the two equivalent circuit is calculated as

$$\boldsymbol{S}_{12} = \begin{bmatrix} 0 & -j\sqrt{\dfrac{d_1^2}{d_1^2+d_2^2}} \\ -j\sqrt{\dfrac{d_1^2}{d_1^2+d_2^2}} & \dfrac{d_2^2}{d_1^2+d_2^2} \end{bmatrix}. \quad \text{(A14)}$$

REFERENCES

[1] C.-L. Chen, W. E. Courtney, L. J. Mahoney, M. J. Manfra, A. Chu, and H. A. Atwater, "A low-loss Ku-band monolithic analog phase shifter," *IEEE Trans. Microwave Theory Tech.*, vol. MTT-35, pp. 315–319, Mar. 1987.

[2] J. F. White, "Diode phase shifters for array antennas," *IEEE Trans. Microwave Theory Tech.*, vol. MTT-22, pp. 658–674, June 1974.

[3] C. E. Free and C. S. Aitchison, "Improved analysis and design of coupled-line phase shifters," *IEEE Trans. Microwave Theory Tech.*, vol. 43, pp. 2126–2131, Sept. 1995.

[4] V. P. Meschanov, I. V. Metelnikova, V. D. Tupikin, and G. G. Chumaevskaya, "A new structure of microwave ultrawide-band differential phase shifter," *IEEE Trans. Microwave Theory Tech.*, vol. 42, pp. 762–765, May 1994.

[5] B. M. Schiffman, "A new class of broad-band microwave 90° phase shifters," *IRE Trans. Microwave Theory Tech.*, vol. MTT-6, pp. 232–237, Apr. 1958.

[6] S. Lucyszyn and I. D. Robertson, "Analog reflection topology building blocks for adaptive microwave signal processing applications," *IEEE Trans. Microwave Theory Tech.*, vol. 43, pp. 601–611, Mar. 1995.

[7] C. Andricos, I. J. Bahl, and E. L. Griffin, "C-band 6 bit GaAs monolithic phase shifter," *IEEE Trans. Microwave Theory Tech.*, vol. MTT-33, pp. 1591–1596, Dec. 1985.

[8] H.-R. Ahn and I. Wolff, "3-dB branch-line hybrid terminated by arbitrary impedances," *Electron. Lett.*, vol. 34, no. 11, pp. 1109–1110, May 1998.

[9] ——, "Arbitrary power division branch-line hybrid terminated by arbitrary impedances," *Electron. Lett.*, vol. 35, no. 7, pp. 572–573, Apr. 1999.

[10] ——, "Asymmetric four-port and branch-line hybrids," *IEEE Trans. Microwave Theory Tech.*, vol. 48, pp. 1585–1588, Sept. 2000.

[11] Y. Yahara, Y. Kadowaki, H. Hoshika, and K. Shirahata, "Broad-band 180° phase shift section in X-band," *IEEE Trans. Microwave Theory Tech.*, vol. MTT-23, pp. 307–309, Mar. 1975.

[12] H.-R. Ahn, I. Wolff, and I.-S. Chang, "Arbitrary termination impedances, arbitrary power division and small-sized ring hybrids," *IEEE Trans. Microwave Theory Tech.*, vol. 45, pp. 2241–2247, Dec. 1997.

[13] H.-R. Ahn and I. Wolff, "Three-port 3-dB power divider terminated by different impedances and its application to MMIC," *IEEE Trans. Microwave Theory Tech.*, vol. 47, pp. 786–794, June 1999.

[14] H.-R. Ahn, I.-S. Chang, and S.-W. Yun, "Miniaturized 3-dB ring hybrid terminated by arbitrary impedances," *IEEE Trans. Microwave Theory Tech.*, vol. 42, pp. 2216–2221, Dec. 1994.

[15] T. Hirota, A. Minakawa, and M. Muraguchi, "Reduced-size branch-line and rat-race hybrids for uniplanar MMIC's," *IEEE Trans. Microwave Theory Tech.*, vol. 38, pp. 270–275, Mar. 1990.

[16] T. Wang and K. We, "Size-reduction and band-broadening design technique of uniplanar hybrid ring coupler using phase inverter for M(H)MIC's," *IEEE Trans. Microwave Theory Tech.*, vol. 47, pp. 198–206, Feb. 1999.

[17] H.-R. Ahn and I. Wolff, "Novel ring filter as a wide-band 180° transmission-line," in *Proc. Eur. Microwave Conf.*, vol. III, Munich, Germany, Oct. 1999, pp. 95–98.

[18] C. Y. Pon, "Hybrid-ring directional coupler for arbitrary power divisions," *IRE Trans. Microwave Theory Tech.*, vol. MTT-9, pp. 529–535, Nov. 1961.

[19] A. K. Agrawal and G. F. Mikucki, "A printed circuit hybrid ring directional coupler for arbitrary power division," *IEEE Trans Microwave Theory Tech.*, vol. MTT-34, pp. 1401–1407, Dec. 1986.

[20] G. F. Mikucki and A. K. Agrawal, "A broad-band printed circuit hybrid ring power divider," *IEEE Trans. Microwave Theory Tech.*, vol. 37, pp. 112–117, Jan. 1989.

[21] H. Hayashi, H. Okazaki, A. Kanda, T. Hirota, and M. Muraguch, "Millimeter-wave-band amplifier and mixer MMIC's using a broad-band 45° power divider/combiner," *IEEE Trans. Microwave Theory Tech.*, vol. 46, pp. 811–818, June 1998.

Hee-Ran Ahn (S'90–M'95–SM'99) received the B.S., M.S., and Ph.D. degrees in electronic engineering from Sogang University, Seoul, Korea, in 1988, 1990, and 1994, respectively, and is currently working toward the Habilitation degree at Gerhard-Mercator University Duisburg, Duisburg, Germany.

From 1991 to 1995, she was a Part-Time Lecturer at Sogang University and a Post-Doctoral Fellow from 1996 to 1997. From February 1997 to October 2001, she was with the Department of Electrical Engineering, Institute of Electromagnetic Field Theory, Gerhard-Mercator University Duisburg. She is currently with the Department of Electrical Engineering, Pohang University of Science and Technology, Pohang, Korea. Her current interests include high-frequency circuit designs.

Ingo Wolff (M'75–SM'85–F'88) was born on September 27, 1938, in Koeslin, Germany. He studied electrical engineering from 1958 to 1964, and received the Dipl.-Ing. degree in electrical engineering, Dr.-Ing. degree in electrical engineering, and Habilitation degree in high-frequency techniques and technologies from the Technical University Aachen, Aachen, Germany, in 1964, 1967, and 1970, respectively.

In 1974, he became the Chair of Electromagnetic Field Theory at Duisburg University, Duisburg, Germany. Since 1999, he has been the President of Duisburg University. In 1992, he founded the Institute of Mobile and Satellite Telecommunications (IMST), Kamp-Lintfort, Germany, a private research institute for wireless communication techniques in which over 110 coworkers are involved in research and development. He is also the Managing Director of the IMST.